New Phytologist

Research

mRNA ADENOSINE METHYLASE promotes drought tolerance through N^6-methyladenosine-dependent and independent impacts on mRNA regulation in Arabidopsis

Diep R. Ganguly[1]*, Yongfang Li[2]*, Susheel Sagar Bhat[1], Shalini Tiwari[2], Pei Jia Ng[2], Brian D. Gregory[1] and Ramanjulu Sunkar[2]

[1]Department of Biology, University of Pennsylvania, Philadelphia, PA 19104, USA; [2]Department of Biochemistry and Molecular Biology, Oklahoma State University, Stillwater, OK 74078, USA

Authors for correspondence:
Brian D. Gregory
Email: bdgregor@sas.upenn.edu

Ramanjulu Sunkar
Email: ramanjulu.sunkar@okstate.edu

Received: *15 July 2024*
Accepted: *5 October 2024*

New Phytologist (2024)
doi: 10.1111/nph.20227

Key words: *Arabidopsis thaliana*, drought, mRNA ADENOSINE METHYLASE, mRNA stability, MTA, N^6-methyladenosine, translation.

Summary

- Among many mRNA modifications, adenine methylation at the N^6 position (N^6-methyladenosine, m^{6}A) is known to affect mRNA biology extensively. The influence of m^{6}A has yet to be assessed under drought, one of the most impactful abiotic stresses.
- We show that *Arabidopsis thaliana* (L.) Heynh. (Arabidopsis) plants lacking mRNA ADENOSINE METHYLASE (MTA) are drought-sensitive. Subsequently, we comprehensively assess the impacts of MTA-dependent m^{6}A changes during drought on mRNA abundance, stability, and translation in Arabidopsis.
- During drought, there is a global trend toward hypermethylation of many protein-coding transcripts that does not occur in *mta*. We also observe complex regulation of m^{6}A at a transcript-specific level, possibly reflecting compensation by other m^{6}A components. Importantly, a subset of transcripts that are hypermethylated in an MTA-dependent manner exhibited reduced turnover and translation in *mta*, compared with wild-type (WT) plants, during drought. Additionally, MTA impacts transcript stability and translation independently of m^{6}A. We also correlate drought-associated deposition of m^{6}A with increased translation of modulators of drought response, such as *RD29A*, *COR47*, *COR413*, *ALDH2B*, *ERD7*, and *ABF4* in WT, which is impaired in *mta*.
- m^{6}A is dynamic during drought and, alongside MTA, promotes tolerance by regulating drought-responsive changes in transcript turnover and translation.

Introduction

Among various abiotic stressors, drought is more widespread in its occurrence and poses a major threat to global crop yields. Alongside an increasing human population, this posits an intensifying need for drought-resilient crops to maintain adequate food production. Drought-induced losses to the production of the four major staple crops in the United States alone has been estimated at $44 billion per year (Razzaq *et al.*, 2021). Much progress has been made toward uncovering the molecular and biochemical pathways underlying stress tolerance (Mickelbart *et al.*, 2015; Chan *et al.*, 2016; Zhu, 2016; Bechtold & Field, 2018). However, genetic manipulation of proteins involved in stress response pathways often entail yield penalties during good seasons (Mickelbart *et al.*, 2015). A promising approach to improve stress tolerance, while minimizing yield penalties, may be to alter the regulation of these pathways (Ganguly *et al.*, 2022). This emphasizes a need for expanding our understanding of the molecular mechanisms promoting drought tolerance.

Abiotic stresses, such as drought, have profound effects on plant growth. Drought triggers a complex signaling cascade that regulates gene expression to facilitate acclimation. Multiple kinases including sucrose nonfermenting1-related protein kinases, mitogen-activated protein kinases, calcium-dependent protein kinases, calcineurin B-like-interacting protein kinases, and receptor-like kinase are integral components of drought signaling (Chen *et al.*, 2021). Likewise, drought-induced signaling compounds, including reactive oxygen species, abscisic acid (ABA), 3′-phosphoadenosine 5′-phosphate, and Ca^{2+}, participate in transducing drought signals (Chan *et al.*, 2016). These signals culminate into the induction of osmotic stress-responsive genes, including *DEHYDRATION-RESPONSIVE ELEMENT-BINDING PROTEINs* (*DREBs*), *ABA-RESPONSIVE ELEMENT-BINDING FACTORs* (*ABFs*), *RESPONSE TO DEHYDRATION 29A* (*RD29A*), and *COLD-REGULATED* (*COR*) genes, many of which drive additional transcriptional changes that help orchestrate downstream drought responses

*These authors contributed equally to this work.

(Yamaguchi-Shinozaki & Shinozaki, 2006; Zhu, 2016; Bechtold & Field, 2018). While much is known regarding transcriptional regulation during drought (Ramanjulu & Bartels, 2002; Yamaguchi-Shinozaki & Shinozaki, 2006; Sunkar *et al.*, 2012), the contribution of RNA modifications is still being elucidated.

Across Eukaryota, mRNA modifications are widespread (often essential) and affect various aspects of mRNA regulation including splicing, stability, and translation. Among those identified so far, methylation of adenosine at position N^6 (m^6A) is the most abundant internal RNA modification (Vandivier & Gregory, 2018; Arribas-Hernández & Brodersen, 2020). It has a characteristic distribution across a transcript, being predominantly enriched in the 3′ untranslated region (UTR) alongside modest enrichment at the start and stop codons (Luo *et al.*, 2014; Prall *et al.*, 2023a). In *Arabidopsis thaliana* (L.) Heynh. (Arabidopsis), the majority of m^6A is deposited by MTA with assistance from accessory proteins mRNA METHYLTRANSFERASE B (MTB), FKBP12 Interacting Protein 37KD (FIP37), VIRILIZER (VIR), and HAKAI (Reichel *et al.*, 2019). MTA, MTB, and FIP37 form the core of the complex and disruption of these components often results in embryo lethality (Bodi *et al.*, 2012; Shen *et al.*, 2016; Růžička *et al.*, 2017). Recently, FIONA1 (FIO1) has also been demonstrated to possess m^6A methyltransferase activity (Sun *et al.*, 2022; Wang *et al.*, 2022; Xu *et al.*, 2022). FIO1 knockout plants show *c.* 10–14% reduction in global m^6A levels and are viable with an early flowering phenotype (Sun *et al.*, 2022; Wang *et al.*, 2022; Xu *et al.*, 2022). m^6A tends to occur in a sequence-specific DRACH (D = A/G/U, R = A/G, H = A/C/U) motif; however, there are multiple observations of its occurrence at a plant-specific UGUA motif (Hu *et al.*, 2021; Govindan *et al.*, 2022; Wang *et al.*, 2022; Sharma *et al.*, 2024). Its presence does not change the sequence context; rather, m^6A affects RNA fate indirectly via changes in secondary structure or the recruitment (or lack thereof) of various proteins (Kierzek & Kierzek, 2003; Liu *et al.*, 2015, 2017; Anderson *et al.*, 2018; Kramer *et al.*, 2020). Notable proteins that can recognize m^6A include 'readers' designated as Evolutionary Conserved C-Terminal Domain (ECT) proteins (Arribas-Hernández *et al.*, 2018; Scutenaire *et al.*, 2018; Wei *et al.*, 2018) and 'erasers' (e.g. AlkB-homology (ALKBH) family proteins) (Mielecki *et al.*, 2012; Duan *et al.*, 2017).

Plant response to stress includes changes in their m^6A topology. For instance, in response to salt stress, m^6A deposition was observed to stabilize salt stress-responsive transcripts via changes in mRNA secondary structure (Anderson *et al.*, 2018; Kramer *et al.*, 2020). A global lack of m^6A (in *vir* mutant) was also shown to result in hypersensitivity to salt stress (Hu *et al.*, 2021). Likewise, VIR-mediated m^6A deposition was important for regulating the translation of photoprotective proteins during high light (Zhang *et al.*, 2022). Similar results were reported from cold and copper-induced oxidative stress, where m^6A-modified transcripts showed increased abundance and ribosome occupancy (Govindan *et al.*, 2022; Sharma *et al.*, 2024). m^6A has also been linked to biotic responses, including viral and bacterial infections (Martínez-Pérez *et al.*, 2021; Prall *et al.*, 2023b). However, the role of MTA and m^6A has yet to be investigated during plant drought stress response. Here, we investigate the extent to which MTA-dependent m^6A dynamics during drought impacts mRNA abundance, translation, and stability to promote drought tolerance in *Arabidopsis*.

Materials and Methods

Plant growth conditions and drought imposition for sequencing

Arabidopsis thaliana (L.) Heynh. Col-0 (wild-type, WT) and *mta* mutants (pro*ABI3:MTA/mta* (Bodi *et al.*, 2012)) were used to conduct experiments. Seeds were planted on soil-filled pots (11 × 9 cm) and kept at 4°C for 3 d for stratification. Seeds were transferred to a growth chamber maintained under 8 h : 16 h, 22°C : 20°C, light : dark for 8 d. Germinated seedlings were then transferred to a growth chamber under a 12 h : 12 h, 22°C : 20°C, light : dark for 9 d. These 17-d-old seedlings were watered to soil capacity, then divided into two groups; watering was withheld for one group in order to progressively induce drought for 12 d, whereas the control group received regular watering. We harvested rosette leaves from *c.* 30–40 plants under control and drought-treated conditions in biological triplicate (biological replicates reflect independently grown plants), which were immediately frozen in liquid nitrogen then stored at −80°C.

Physiological assays and drought phenotyping

For phenotyping, plants were drought-stressed as described above, except that water was withheld for between 21 and 27 d. After this, between the 21st and 27th day of stress, one pot at a time was rewatered each consecutive day and allowed to grow to assess recovery.

Electrolyte leakage was assessed in WT and *mta* under control and drought conditions to compare drought tolerance as described previously (Govindan *et al.*, 2022). Briefly, seven replicates of two fully developed rosette leaves were excised from drought-stressed WT and *mta* plants and placed in 20 × 150 mm tubes containing 100 µl of deionized water. Then, 12 ml of deionized water was added to each tube followed by gentle shaking overnight at room temperature. Solution conductivity was measured using a conductivity meter (Orion Star A212; Thermo Fisher Scientific, Carlsbad, CA, USA). Next, the samples were autoclaved at 121°C for 20 min, and then agitated for 2 h before measuring conductivity again. The percentage of electrolyte leakage was calculated as the ratio of conductivity before and after autoclaving.

Proline content was analyzed as described previously (Carillo & Yves, 2011). The ethanolic extract was prepared by homogenizing *c.* 100 mg leaves in 1 ml of 70% ethanol. The 100 µl reaction mixture constituted 1% (w/v) ninhydrin in 60% (v/v) acetic acid and 20% (v/v) ethanol, mixed with 50 µl of ethanolic extract. The reaction mixture was then incubated at 95°C for 20 min, cooled to room temperature, and absorbance was recorded at 520 nm in a microplate reader.

Data shown represent means and SD from three biological and nine technical replicates. Analysis of variance and *post hoc* Tukey's test was used to test for significant differences.

RNA isolation and poly(A) selection

Total RNA was extracted using TRIzol reagent (Thermo Fisher Scientific). The quantity and integrity of total RNA were measured using a Nanodrop ND-1000 (Thermo Fisher Scientific) and gel electrophoresis, respectively. Approximately 170 μg total RNA was used for poly(A) RNA isolation using the Dynabeads mRNA Purification Kit (Invitrogen). The mRNA-seq, m^{6}A-IP-seq, and GMUCT libraries were produced using the same RNA for each sample.

m^{6}A-RNA immunoprecipitation and library preparation

Approximately 1.5 μg of poly(A) RNA (mRNA) was chemically fragmented with the NEBNext Magnesium RNA Fragmentation Module (NEB, Ipswich, MA, USA). Fragmented mRNA was used for m^{6}A-IP using the EpiMark N6-Methyladenosine Enrichment Kit (NEB) and 10% was kept, before IP, as the input control. Libraries from input mRNA and immunoprecipitated RNA (m^{6}A-IP) were prepared with the NEBNext Ultra II Directional RNA Library Prep Kit for Illumina (NEB).

Polysomal RNA library preparation

Polysomes were isolated as previously described (Li *et al.*, 2017; Govindan *et al.*, 2022). Harvested leaf tissue was ground into a fine powder in liquid nitrogen. Approximately 1.25 ml of polysome extraction buffer (200 mM Tris-Cl (pH 9.0), 200 mM KCl, 26 mM $MgCl_2$, 25 mM EGTA, 100 μM 2-mercaptoethanol, 50 μg ml^{-1} cycloheximide, 50 μg ml^{-1} chloramphenicol, 1% Triton X-100, 1% Brij-35, 1% Tween-40, 1% IGEPAL CA-630, 2% polyoxyethylene (10) tridecyl ether, 1% deoxycholic acid) was added to the powdered tissue (500 mg), mixed thoroughly, and then incubated on ice for 10 min with occasional mixing by inversion. The mixture was centrifuged at 4°C for 2 min at 16 900 ***g***. Approximately 600 μl of supernatant was layered onto the top of a sucrose gradient (20–60% sucrose, w/v) and centrifuged for 120 min at 275 000 ***g*** in an Optima LE-80 centrifuge (Beckman, Indianapolis, IN, USA). The optical density of the gradient fractions was measured by using a UA-5 detector and a Gradient Fractionator (model 640; ISCO) at 254 nm. Sucrose fractions with more than two ribosomes were pooled and used for polysomal RNA isolation using TRIzol reagent. Approximately 8 μg of polysomal RNA was used for mRNA purification, which was then used for library construction using the KAPA Stranded mRNA-seq Kit.

RT-qPCR

First-strand cDNA synthesis was performed with 2 μg of DNase-treated (DNase I; Invitrogen) RNA using Superscript reverse transcriptase II (Invitrogen). PCRs were performed in the total volume of 10 μl, with 0.5 μM of each forward and reverse primers and 2× Power SYBR Green PCR mix (Applied Biosystems, Waltham, MA, USA) on a LightCycler 96 system (Roche). The PCR conditions included an initial denaturation at 96°C for 1 min, followed by 40 cycles of 5 s at 94°C and 1 min at 60°C. The PCR was performed on two independent biological samples with two technical replicates. The relative expression levels of the target genes were calculated using $2^{-\Delta\Delta Ct}$ (Livak & Schmittgen, 2001) and normalized against *PP2AA3* (*AT1G13320*). Primers are listed in Supporting Information Table S1.

GMUCT

GMUCT libraries were constructed as previously described (Willmann *et al.*, 2014) using 600 ng poly(A) RNA.

Sequence analysis

A full description of the sequencing analyses performed is provided in the Methods S1. All code used for analyses are available on GitHub (https://github.com/dtrain16/NGS-scripts). Sequencing statistics are summarized in Table S2.

Results

MTA contributes to drought tolerance

To investigate whether MTA contributes toward drought tolerance, we compared drought sensitivity between wild-type Col-0 (WT) and a line with embryo-specific expression of *MTA* (pro*ABI3*:*MTA*/*mta* herein referred to as *mta*) that is required for these *mta* mutant plants to properly progress through embryonic development (Bodi *et al.*, 2012). We imposed drought on 17-d-old WT and *mta* plants by withholding water for up to 27 d followed by rewatering to evaluate recovery (Fig. 1a,b). After 21 d, WT and *mta* showed 100% and 38% recovery, respectively (Fig. 1b). This decreased to 91% and 14% in WT and *mta* plants, respectively, after 23 d. None of the *mta* plants could recover after 25 d, whereas *c.* 30% of WT plants could recover. We also characterized drought sensitivity using physiological assays. First, we measured electrolyte leakage as a measure of damage to the plasma membrane. Under control conditions, ion leakage was comparable between WT and *mta*. However, *mta* displayed significantly higher levels of leakage (72%), compared with WT (46%), under drought (Fig. 1c). We next evaluated proline accumulation, a drought-induced solute considered to act as an osmoprotectant (Ramanjulu & Sudhakar, 2000; Bartels & Sunkar, 2005). While proline levels were elevated in both WT and *mta* plants under drought, the level of accumulation was significantly lower in *mta* (Fig. 1d). We also evaluated changes in *MTA* transcript abundance, in both total mRNA and polysomal RNA fractions, in WT and *mta* under drought (Fig. 1e). This was especially important since *MTA* is under the control of the drought-inducible *ABI3* promoter in the *mta* mutant. In WT, we observed a subtle decrease of *MTA* in the total mRNA pool under drought; however, *MTA* levels

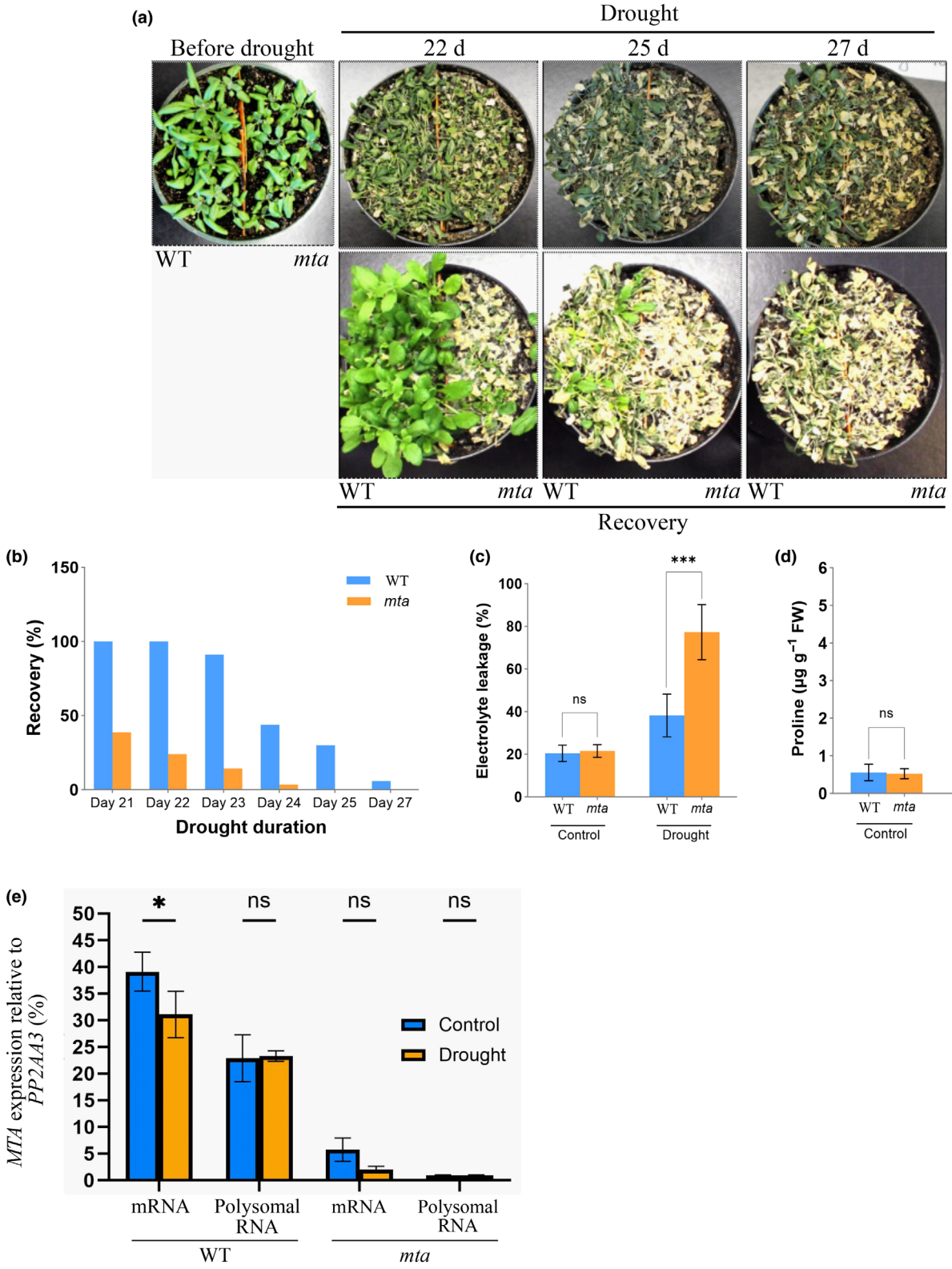

Fig. 1 mRNA ADENOSINE METHYLASE (MTA) is important for drought tolerance in Arabidopsis. (a) Phenotype of wild-type (WT) (Col-0, left) and *mta* (pro*ABI3*::*MTA*/*mta*, right) plants before, during, and after drought. (b) Percent of WT and *mta* plants that were viable after rewatering following drought. (c, d) Electrolyte leakage (c) and proline (d) quantification in WT and *mta* following 21 d of drought. (e) Relative expression of *MTA* in total and polysomal mRNA after 12 d of drought as determined by reverse transcription quantitative polymerase chain reaction. Expression level is normalized to *PP2AA3* (*AT1G13320*). Data are shown as mean and SD. Statistical significance denoted by: ns, $P > 0.05$; *, $P < 0.05$; **, $P < 0.01$; ***, $P < 0.001$; ****, $P < 0.0001$.

were unchanged in the polysomal RNA fraction. Importantly, in *mta*, we observed substantially reduced expression of *MTA* in the total mRNA pool and negligible levels in the polysomal RNA fraction. Furthermore, *MTA* expression was not induced under drought in *mta*. Taken together, *mta* mutants exhibit attenuated expression of *MTA*, which correlates with increased drought sensitivity.

m^{6}A dynamics during drought

To study m^{6}A dynamics during drought, we performed m^{6}A-RNA immunoprecipitation sequencing (m^{6}A-RIP-seq) on WT and *mta* plants subjected to 12 days of drought (DT) along with control (CK) plants. We confirmed data reproducibility through multidimensional scaling analysis (MDA) (Fig. S1A). We observed separation by condition (PC1) and genotype (PC2), suggesting that these were the primary sources of variation in m^{6}A across our samples. We then calculated transcriptome-wide m^{6}A enrichment across all samples (Fig. 2a). In WT under CK conditions, we observed m^{6}A to be highly enriched throughout the 3′ UTR with relatively modest, yet pronounced, levels at the start and stop codons, which is consistent with previous observations (Luo *et al.*, 2014). Compared with WT, *mta* exhibits a substantial depletion of m^{6}A largely at the stop codon and throughout the 3′ UTR. Interestingly, transcripts in *mta* plants showed higher levels of m^{6}A in both the 5′ UTR and CDS than WT, which may reflect altered activity of other m^{6}A regulators, including FIO1 and m^{6}A erasers, in the absence of MTA (herein referred to as compensatory regulation). In WT, DT was associated with hypermethylation at the start and stop codons, within the CDS, and across the 3′ UTR, while hypomethylation was observed in the 5′ UTR. Interestingly, *mta* showed similar m^{6}A changes to WT in the 5′ UTR (hypomethylation) and stop codon (hypermethylation) under DT. However, *mta* also showed hypo-methylation within the CDS and, critically, no change in m^{6}A at the start codon and throughout the 3′ UTR during DT. These observations suggest that m^{6}A deposition is likely to be regulated during DT in both an MTA-dependent and -independent manner. Our results link MTA to DT-induced hypermethylation within the CDS and the 3′ UTR (as observed in WT), whereas MTA-independent changes (observed in *mta*) may reflect compensatory regulation that occurs when MTA function is disrupted.

To investigate transcript-specific changes in m^{6}A, we employed MACS2 to identify regions enriched for m^{6}A. We considered high-confidence peaks as those detected in all three biological replicates for each genotype and condition (Fig. S1B). A total of 6213, 8472, 5344, and 5349 high-confidence peaks were identified across WT and *mta* in CK and DT, respectively (Table S3). Visualizing m^{6}A levels at these sites revealed complex patterns of change between genotypes and conditions (Fig. S1C). Consistent with the global trend, there were a large proportion of sites showing hypermethylation in WT under DT. On the other hand, while *mta* showed overall depletion in m^{6}A, there were still clusters of sites where hypermethylation still occurred, possibly reflecting FIO1 or m^{6}A eraser activity. However, this induction appears insufficient to recapitulate WT levels of m^{6}A under DT at the majority of sites.

Since *mta* is drought-sensitive, we reasoned that MTA-induced hyper-methylation may contribute to DT tolerance. To investigate transcript-specific regulation of m^{6}A by MTA, we adopted a strategy to focus on regions with m^{6}A peaks in WT, but not *mta*, which we term MTA-affected sites (Fig. 2b) (Prall *et al.*, 2023b). We identified 2697 and 4233 such sites in CK and DT, respectively, which formed the basis for further analysis (Table S4). Of these peaks, 1270 out of 5660 (22.4%) were detected in both conditions while 1427 (25.2%) and 2963 (52.3%) were observed specifically under CK or DT, respectively. These latter peaks correspond to 1370 and 2674 transcripts in CK and DT, respectively. Testing for enriched motifs within MTA-affected sites revealed the plant-specific UGUA motif that has been repeatedly identified (Luo *et al.*, 2020; Govindan *et al.*, 2022; Wang *et al.*, 2022; Prall *et al.*, 2023b; Sharma *et al.*, 2024). This motif was highly prevalent (69.2%) amongst MTA-affected sites under DT (Fig. 2b). We also identified the motifs GAAGAA and UAUAUA among hypomethylated and hypermethylated targets, respectively, albeit at a lower proportion than UGUA.

Hierarchical clustering of MTA-affected sites revealed five clusters of interest (Fig. 2c). These clusters were enriched for sites that were hypo- (I, II) or hyper-methylated (III, V) during DT in WT, with reduced m^{6}A levels in *mta* plants. Cluster IV also showed a bias toward hypermethylation during DT in WT alongside a subset of hypomethylated sites that were difficult to separate without forming an excessive number of clusters. Despite the overall reduction in m^{6}A levels in *mta*, clusters III and IV showed comparable fold-changes in m^{6}A, between CK and DT, in WT and *mta*, which may reflect compensatory regulation. Similarly, Cluster I, which had a bias of hypomethylated sites under DT in WT, were hypermethylated under DT in *mta*. Conversely, Clusters II and V contained hypo- and hypermethylated sites in WT, respectively, without m^{6}A changes in *mta*. Although both sets of sites display an overall reduction in m^{6}A in *mta*, the DT-responsive m^{6}A status of Cluster V sites seem to be primarily governed by MTA activity, whereas secondary regulation may be occurring at Cluster III sites.

We next considered the location of MTA-dependent m^{6}A sites, which predominantly occurred (> 75%) within the 3′ UTR of protein-coding transcripts (Fig. 2d). This was consistent across each cluster of MTA-affected m^{6}A sites. We next explored the biological functions of the proteins encoded by transcripts overlapping with m^{6}A sites, from each cluster, by testing for over-represented GO terms using PANTHER (Mi *et al.*, 2019). The strongest enrichments were observed for higher level (or parent) GO terms, related to primary metabolism and cellular processes (Fig. 2e). These were evident across all clusters of m^{6}A sites, although they were most pronounced in Clusters III and IV. Importantly, we also observed enriched terms related to photosynthesis and stress in specific clusters. For example, response to salt stress and proteolysis were evident amongst transcripts overlapping with Cluster II sites (hypomethylated),

whereas response to abiotic stimulus, photosynthesis, and chloroplast organization was found in transcripts overlapping with Cluster III sites (hypermethylated). We also observed terms related to mRNA processing and gene expression in Cluster IV (hypermethylated). Collectively, this suggests that while m^{6}A is regulated on a suite of transcripts associated with core cellular

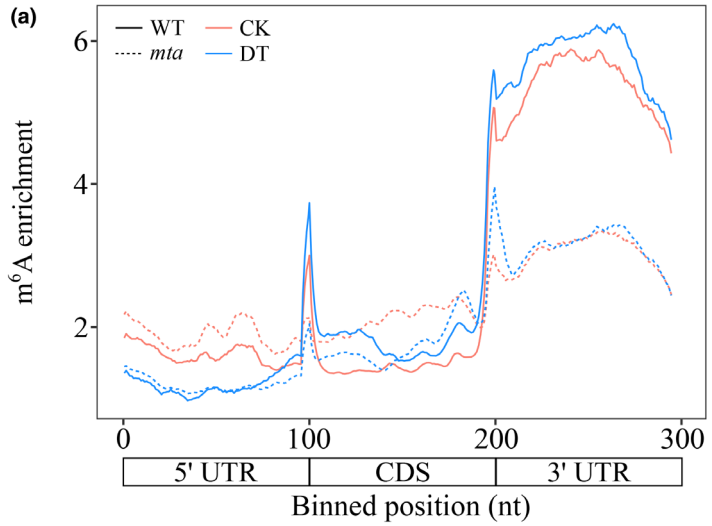

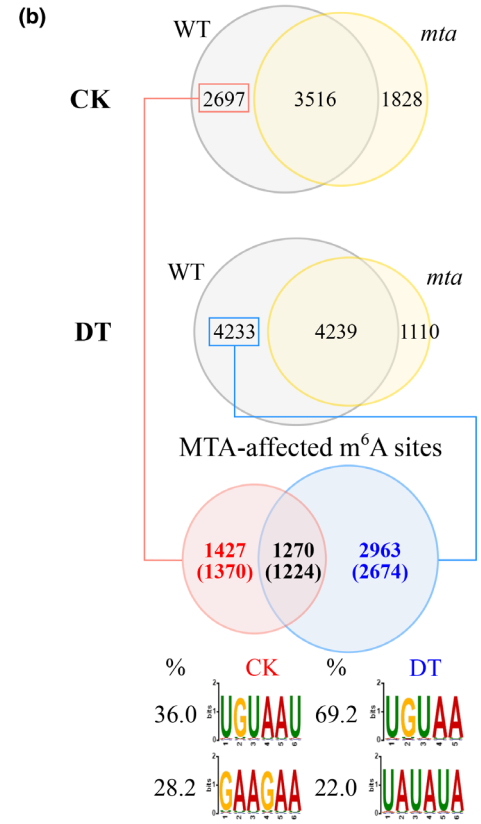

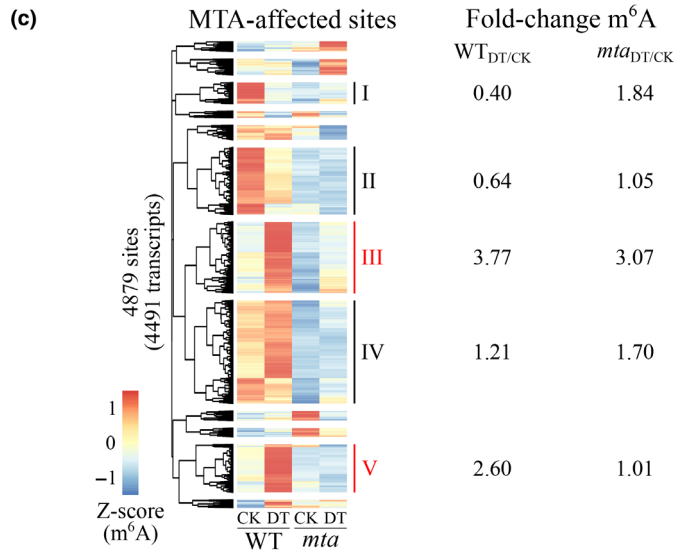

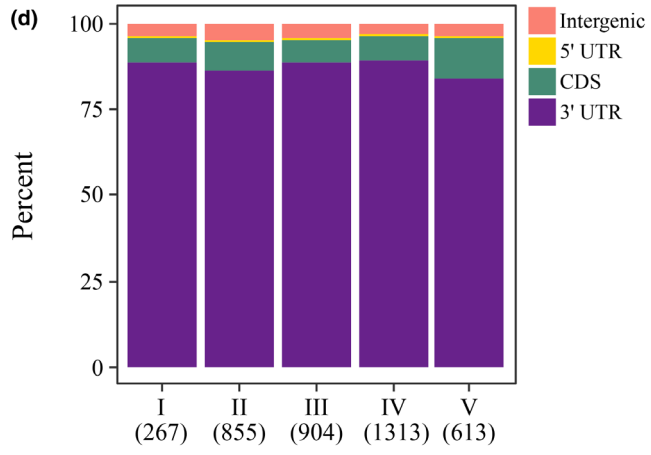

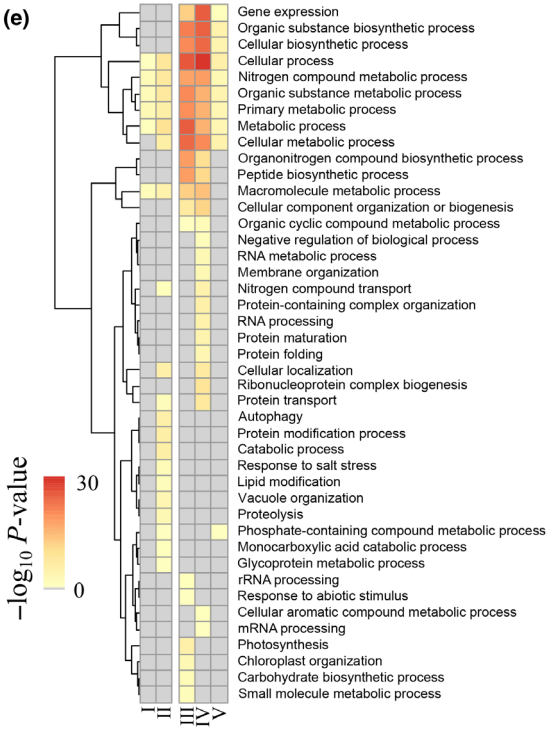

Fig. 2 RNA m6A is remodeled during drought in Arabidopsis. (a) m^6A enrichment (RPM_{IP}/RPM_{input}), binned into 10 nt rolling windows, across all detected transcripts. (b) Venn diagrams representing the number of high-confidence m^6A peaks identified in wild-type (WT) and *mta* under CK and DT. mRNA ADENOSINE METHYLASE (MTA)-affected sites were defined as those detected only in WT. Numbers in brackets denote number of unique overlapping genes. Enriched motifs were identified using STREME. (c) Heatmaps with one-dimensional hierarchical clustering of rows representing m^6A enrichment, scaled as row-wise Z-scores, at MTA-affected sites. Roman numerals denote cluster and the mean fold-change in m^6A under DT, among sites within each cluster, is shown for WT and *mta*. (d) Proportion of MTA-affected m^6A sites occurring within a 5′ UTR, CDS, 3′ UTR, or intergenic region. Number in brackets represents the number of m^6A sites in each cluster. (e) Over-represented GO terms among protein-coding genes harboring MTA-dependent m^6A sites. Gray denotes nonsignificant (*P*-value > 0.05) terms.

functions, DT-induced changes in m^6A are found on stress-related transcripts in their 3′ UTR.

Impacts of MTA and m^6A on drought-responsive changes in mRNA abundance

The presence of m^6A has been linked to various aspects of mRNA regulation, including stability and translation (Prall *et al.*, 2023a). Therefore, we hypothesized that the altered m^6A regulation in *mta* could influence the abundance, stability, or translation of stress-related transcripts, leading to drought sensitivity. Additionally, since there may be multiple impacts on mRNA regulation, we first highlight the changes that can be attributed to lack of MTA before evaluating the extent to which these changes can be directly associated with changes in m^6A, or not, as measured by our m^6A-RIP-seq. We consider this strategy to more precisely capture the impact of m^6A on mRNA regulation.

We first investigated DT-responsive changes in mRNA abundance. When directly comparing differential expression during DT, we observed a significant overlap between WT and *mta* (Fig. S2A,B; Table S5). For both genotypes, the DT-responsive transcripts were enriched for functions related to stress response, including water deprivation and abscisic acid (Fig. S2C). Although a significant proportion of the same transcripts are DT-responsive in both genotypes, it is not clear whether this is occurring to the same magnitude. We identified 2725 such transcripts with altered DT-responsive abundance changes with a bias (1731, 63.5%) toward larger increases in abundance in *mta* compared with WT (Fig. 3a). Within this collection of transcripts, we observe a striking over-representation of functional terms related to stress response (Fig. 3b). These results suggest that *mta* exhibits larger increases in mRNA abundance of stress-associated transcripts, which may reflect its increased sensitivity to DT.

Next, we assessed the extent to which changes in mRNA abundance in *mta* was correlated with changes in m^6A either constitutively or under DT. To test the former, we compared mRNA abundance, measured under CK, between transcripts with and without MTA-affected m^6A sites (Fig. 3c). We observed a bias toward increased abundance for transcripts harboring a MTA-affected m^6A site compared with those that did not. Interestingly, although statistical significance was achieved, we observed highly comparable transcript abundances between WT and *mta* for each fraction. For transcripts harboring MTA-affected m^6A sites in WT under CK, we utilized linear modeling to relate m^6A levels to mRNA abundance. Counterintuitively, we observed that m^6A was moderately anticorrelated with mRNA abundance (adjusted $R^2 = 0.24$, slope = −0.47, Pearson's $r = -0.49$, Fig. S3A). We then interrogated whether m^6A dynamics could influence DT-responsive changes in mRNA abundance. Since there is a global trend toward hypermethylation, and MTA activity facilitates m^6A deposition, we reasoned that Clusters III (904 m^6A peaks, 854 transcripts) and V (613 m^6A peaks, 586 transcripts) provide an ideal subgroup of sites with which to reveal the regulatory consequences of attenuated m^6A regulation in *mta* (Fig. 2c). Hence, we compared the DT-induced fold-changes between WT and *mta* in transcripts with Cluster III or V MTA-affected m^6A sites (Fig. 3d). Interestingly, for transcripts with Cluster V sites, a small but statistically significant increase in fold-change was observed in *mta*. Taken together, these results suggest that while MTA has a substantial impact on DT-responsive changes in stress-related transcript abundance, m^6A has a relatively minor contribution to a subset of transcripts.

MTA impacts RNA turnover and drought-responsive changes in transcript stability is influenced by m^6A

Since m^6A has been reported to stabilize mRNAs (Anderson *et al.*, 2018), we interrogated the extent to which MTA-affected m^6A changes impacted transcript stability. For this, we performed global mapping of uncapped and cleaved transcripts (GMUCT) (Willmann *et al.*, 2014). This method profiles 5′-monophosphorylated RNAs (i.e. uncapped mRNAs) representing transcripts undergoing 5′-end decay, allowing for inferences on mRNA turnover and stability. Our quality control analysis using MDA revealed high reproducibility (86%, Fig. S4A), and we observed 3-nucleotide phasing with a bias for the translational frame (frame 0, Fig. S4B) as previously reported (Hou *et al.*, 2016; Yu *et al.*, 2016). In order to assess differences in cotranslational decay, we summarized 5′-P end accumulation based on the position of the 5′ edge of a terminating ribosome (17 nucleotides upstream of the stop codon) as previously described (Hou *et al.*, 2016; Yu *et al.*, 2016). For each genotype, DT-treated samples showed higher accumulation of 5′-P ends, whereas *mta* mutants had higher accumulation of 5′-P ends than WT in both CK and DT conditions. However, when expressed as a percentage of the total 5′-P ends at each transcript (relative frequency of 5′-P ends, see Supporting Information (Lee *et al.*, 2020)), we observed highly comparable signatures between genotypes and conditions (Fig. 4b). This suggests that there is a

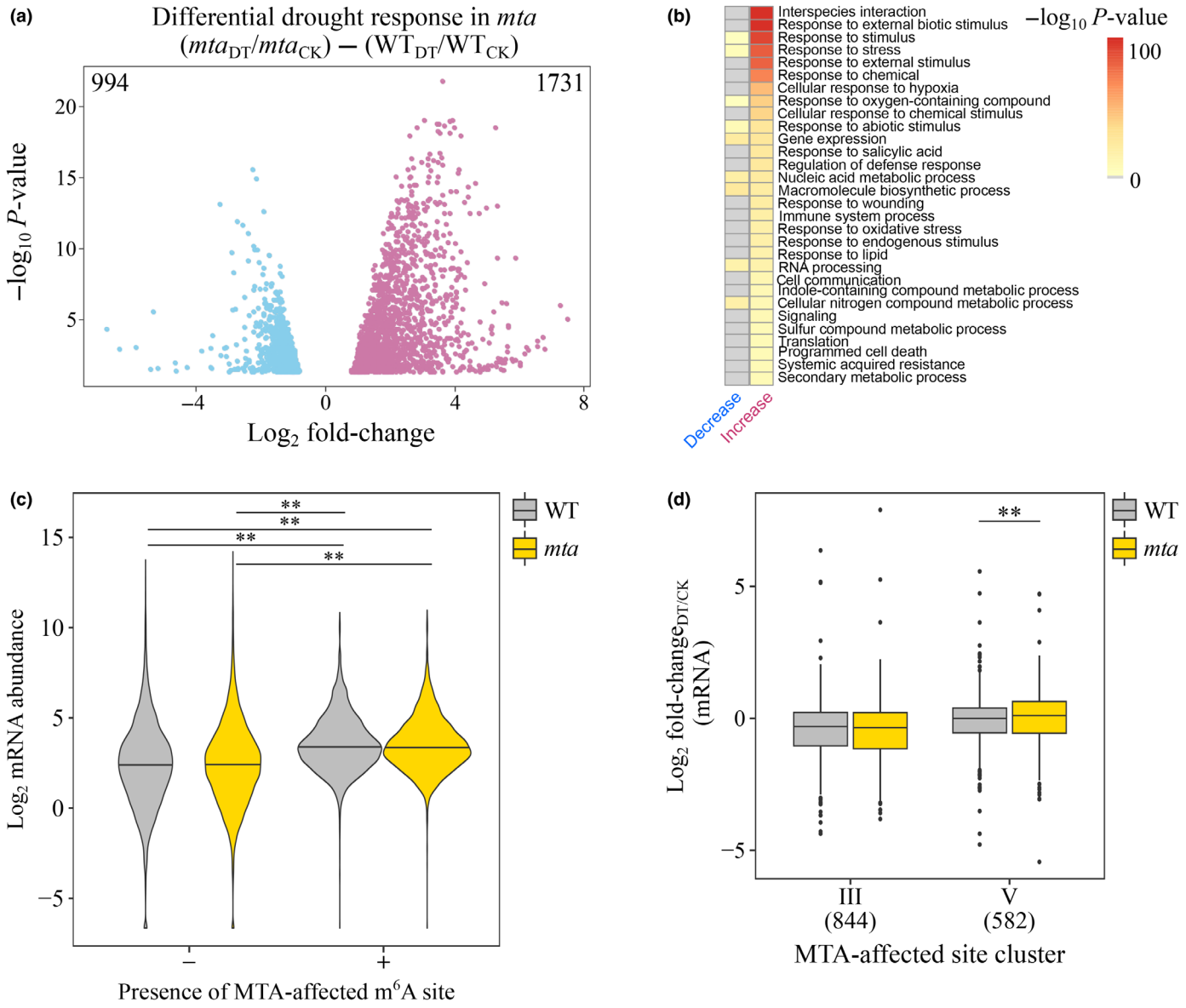

Fig. 3 Assessing the impacts of mRNA ADENOSINE METHYLASE (MTA) and m^{6}A on drought-responsive changes in mRNA abundance in Arabidopsis. (a, b) Volcano plot of (a), and over-represented GO terms in (b), genes with differential DT-responsive changes in mRNA abundance in *mta*. Gray denotes nonsignificant GO terms. (c) Violin plot of $\log_2$ mRNA abundance in wild-type (WT) and *mta* (CK only) for transcripts with (+) or without (−) a MTA-affected m^{6}A site. Horizontal line denotes median. (d) Standard boxplots of $\log_2$ fold-changes in mRNA abundance, in WT and *mta*, for transcripts that contain a MTA-affected m^{6}A site from Cluster III or V. Horizontal lines denote the first (bottom), second (median, middle), and third quartiles (top). Whiskers denote 1.5× interquartile range. Data outside the interquartile range are denoted as circles. Numbers denote the number of genes detected for each category. Statistical significance was determined using Dunn's test of multiple comparisons with *P*-values adjusted using the Bonferroni method: **, $P < 0.01$; *, $P < 0.05$.

global increase in RNA turnover, as opposed to specific changes in ribosome stalling or cotranslational RNA decay, when MTA is disrupted and during DT conditions.

We then assessed the impact of MTA on differential accumulation of uncapped RNAs, relative to total mRNAs, in a transcript-specific manner by combining our GMUCT and mRNA-seq datasets (Tables S5, S6). Interestingly, there were a greater number of transcripts with significant changes in the levels of uncapped RNAs, compared to mRNAs, with a bias toward an increased abundance (Fig. S4C). This aligns with the global trend of increased uncapped RNAs, reinforcing a link between MTA and RNA turnover. We then interrogated changes under DT, which induced changes in uncapped RNAs for 7185 and 5690 transcripts in WT and *mta*, respectively. Importantly, we identified 2306 mRNAs with differential DT-induced changes in uncapped RNAs in *mta* of which 637 occurred without a significant change in total mRNA (Fig. 4c). We tested for over-represented GO terms amongst these transcripts and observed an enrichment for stress-related terms, especially for those with altered DT-responsiveness in both mRNA and uncapped RNA (Fig. 4d). This suggests that MTA impacts DT-induced changes in the turnover of stress-related transcripts.

We next investigated the extent to which transcript stability was associated with perturbed m^{6}A in *mta* mutants. To facilitate associating changes in m^{6}A with those in transcript stability, while accounting for transcription, we utilize the proportion uncapped metric ($GMUCT_{RPM}/mRNA_{RPM}$) where an increase in proportion uncapped equates to reduced stability (Vandivier *et al.*, 2015) and vice versa. We first considered the steady-state relationship between m^{6}A and transcript stability. A small, but significant, decrease in proportion uncapped was observed in transcripts with an MTA-affected m^{6}A site compared to those without (Fig. 4e). However, as with mRNA abundance, proportion uncapped was highly comparable between genotypes for transcripts with and without an MTA-affected m^{6}A site. Furthermore, linear regression revealed a negligible relationship between m^{6}A and proportion uncapped in WT samples under CK conditions (adjusted $R^2 = 1.5 \times 10^{-4}$, slope = 0.01, Pearson's $r = 0.01$, Fig. S3B). These results suggest that m^{6}A has a minor contribution toward steady-state transcript stability at a transcriptome-wide level.

We then tested how m^{6}A impacts transcript stability during DT by comparing the DT-induced fold-changes in proportion uncapped, between WT and *mta*, for transcripts harboring Cluster III and V MTA-affected m^{6}A sites (Fig. 2c; Table S7). While transcripts with Cluster III sites did not show a significant difference in proportion uncapped, those with Cluster V sites had a significantly lower median value in *mta* compared with WT (Fig. 4f). This analysis suggests that those transcripts that are no longer methylated during DT in *mta* mutants (Cluster V sites) have a lower change in proportion uncapped, corresponding to a reduced destabilization (or relatively higher stability). On the other hand, sites at which m^{6}A was attenuated in *mta* but displaying DT-responsive hypermethylation (Cluster III sites) showed comparable stability changes between genotypes. Together, this suggests that m^{6}A dynamics has a minor role in influencing transcript stability during DT.

m^{6}A promotes increased polysome occupancy for a subset of stress-associated transcripts during drought

m^{6}A has been documented to influence translation in plants (Luo *et al.*, 2020; Zhou *et al.*, 2021; Govindan *et al.*, 2022; Sharma *et al.*, 2024). Therefore, we utilized polyribosome (polysome)-associated RNA-sequencing to investigate the impacts of m^{6}A on DT-induced changes in translation (Li *et al.*, 2017). MDA revealed high reproducibility with DT being the primary source of variation (PC1 = 88%) between samples followed by genotype (PC2 = 9%, Fig. S5A). We then interrogated changes in polysomal RNA relative to changes in total mRNA (Tables S5, S8). Examining *mta* under CK conditions, there was a striking bias toward changes in the polysomal RNA fractions compared with total mRNA (as measured from input mRNA samples), highlighting that MTA-mediated m^{6}A deposition has greater impacts posttranscriptionally (Fig. S5B). To explore the extent to which these occur under DT, we compared changes in the total and polysomal RNA fractions between WT and *mta* (Fig. 5a). Once again, there was a striking bias toward changes observed in the polysomal RNA fraction. Of interest, was the enrichment of stress-associated transcripts whose association to polysomes were impacted (Fig. 5b). As expected, there was a significant enrichment of transcripts associated with stress responses, including response to water and oxidative stress. This enrichment was most evident among transcripts with altered polysomal RNA abundance as compared to changes in their overall mRNA abundance. This suggests that MTA is important for polysome association, especially for stress-related transcripts during DT.

We then evaluated whether the impacts in polysome association in *mta* could be associated with changes in m^{6}A. We combined our polysomal RNA- and mRNA-seq data to compute transcript-specific polysome occupancy for evaluating changes in polysome association that are independent of changes in total mRNA (Table S9). Under steady state, we again observe a small, but significant, difference in polysome occupancy in transcripts that contain an MTA-affected m^{6}A site compared to those without (Fig. 5c). Similarly, abundances between genotypes, for both transcript fractions, were comparable despite statistical significance. Linear modeling revealed a negligible relationship between m^{6}A levels and polysome occupancy amongst transcripts harboring an MTA-affected m^{6}A site (adjusted $R^2 = 6.1 \times 10^{-3}$, slope = −0.03, Pearson's $r = 0.08$, Fig. S3C). We then associated m^{6}A status to DT-induced changes in polysome occupancy for transcripts harboring Clusters III and V m^{6}A sites (Fig. 2c). A statistically significant decrease in DT-induced fold-changes in polysome occupancy was observed in transcripts with Cluster V sites (Fig. 5d). This analysis aligns with results obtained regarding the proportion of uncapped transcripts suggesting that, although steady-state m^{6}A levels have a negligible relationship with polysome occupancy, changes in m^{6}A influence the regulation of transcript-specific translation during DT.

Validation of translational regulation of drought-associated transcripts by MTA and correlation with m^{6}A

Our sequencing-based analysis links DT-associated changes in m^{6}A with subtle impacts on the abundance, stability, and translation of transcripts largely associated with metabolic and gene regulatory processes (Cluster V, Fig. 2e). We further explored our polysomal RNA-sequencing dataset for evidence of altered translation of drought-related transcripts. We found several important drought-associated genes that had attenuated regulation in *mta*, including *RD29A*, *COR47*, *COR413*, *ALDEHYDE DEHYDROGENASE 2B* (*ALDH2B*), *EARLY RESPONSE TO DEHYDRATION 7* (*ERD7*), and *ABF4* (Tables S8, S9). Consistent with our analysis of polysome occupancy (Fig. 5d), we observed weaker DT-responsive changes in polysomal RNA abundance in *mta*, compared with WT plants for many DT-relevant genes including *RD29A*, *COR413*, *COR47*, *ALDH2B*, *ERD7*, and *ABF4* (Fig. 6). Impaired translation of such transcripts may explain why *mta* is drought-sensitive. We corroborated three of these observations (*RD29A*, *COR47*, and *COR413*) using quantitative reverse transcription polymerase chain reaction on total and polysomal RNA fractions (Fig. 7a).

Additionally, given the importance of DREBs in plant drought responses, we measured *DREB1B*, *DREB1C*, and *DREB1A* along with *COR15A* and *KIN1* (targets of DREBs) in WT and *mta* plants during DT. All these transcripts displayed significantly reduced DT-responsive fold-changes in the polysomal RNA fraction in *mta* compared with WT (Fig. 7a).

A limitation in our analysis is that many critical modulators of drought, such as the DREBs, were not captured as an

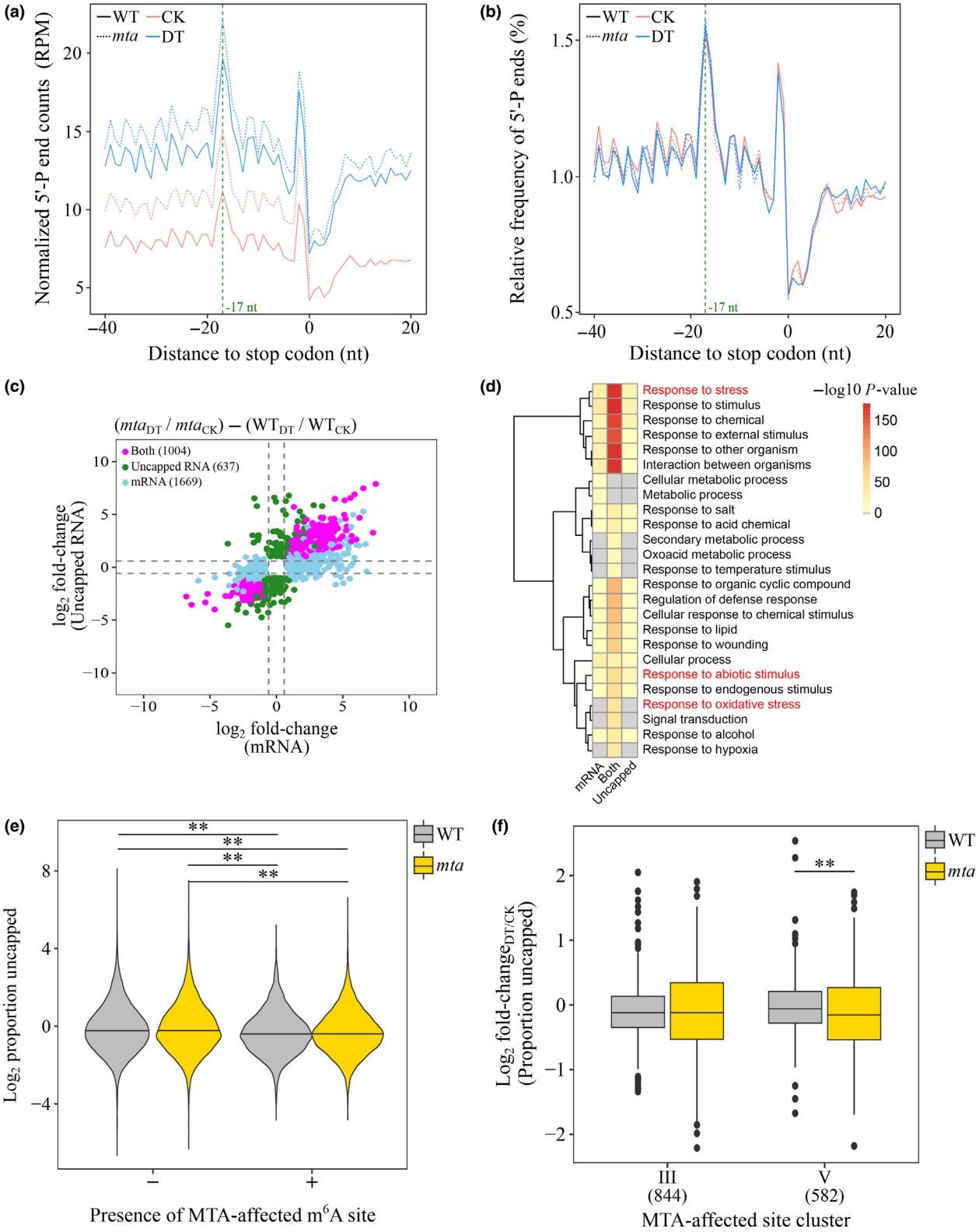

Fig. 4 mRNA ADENOSINE METHYLASE (MTA) influences global RNA turnover and m^{6}A dynamics influence DT-responsive changes in transcript stability in Arabidopsis. (a, b) Mean normalized (a) and relative frequency (b) of 5′-P ends relative to stop codons. Dotted line represents the 5′ edge of a ribosome 17 nucleotides upstream of a stop codon at the A site. (c, d) Scatter plot of changes in uncapped and input mRNA (c), and over-represented GO terms (d), for genes with differential DT response in *mta*. Colours denote statistically significant changes in input mRNA (blue), uncapped mRNA (green), or both (magenta). (e) Violin plot of $\log_2$ proportion uncapped in wild-type (WT) and *mta* (CK only) for transcripts with (+) or without (−) a MTA-affected m^{6}A site. Horizontal line denotes median. (f) Standard boxplots of $\log_2$ fold-changes in proportion uncapped during DT, in WT and *mta*, for transcripts that contain a MTA-affected m^{6}A site from Cluster III or V. Horizontal lines denote the first (bottom), second (median, middle), and third quartiles (top). Whiskers denote 1.5× interquartile range. Data outside the interquartile range are denoted as circles. Numbers denote the number of genes detected for each category. Statistical significance was determined using Dunn's test of multiple comparisons with *P*-values adjusted using the Bonferroni method: **, $P < 0.01$; *, $P < 0.05$.

MTA-affected m^{6}A site. Since these transcription factors are DT-responsive, we reasoned that this may be due to DT-induced transcription reducing the m^{6}A enrichment at these genes (determined by MACS2), thereby decreasing peak calling sensitivity. In our data, increased polysomal RNA abundance, under DT, was evident in WT alongside a concomitant increase in m^{6}A (Fig. 6). Conversely, in *mta*, where m^{6}A levels are visibly lower, a weakened induction under DT was observed. This suggests that m^{6}A changes are occurring at transcripts important for drought and contribute to their regulation at the level of translation. To further quantify this, we extracted m^{6}A enrichment, mRNA abundance, proportion of uncapped transcripts, and polysome occupancy for the abovementioned genes, as well as genes related to proline metabolism (Fig. 7b). Counterintuitively, many of these transcripts had higher levels of m^{6}A in *mta*, again potentiating compensatory feedback by other m^{6}A machinery. Regardless of overall m^{6}A, many transcripts demonstrated DT-induced hypomethylation, which opposes the global trend toward hypermethylation. This suggests that these transcripts are generally methylated by MTA, however, are subject to secondary m^{6}A regulation during DT. Most of these transcripts showed comparable changes in mRNA abundance between genotypes, which likely reflects that these were driven by DT-induced transcription. There was also a combination of DT-induced changes in the proportion of uncapped transcripts and polysome occupancy that were in opposing directions (e.g. *COR47*). On the other hand, *mta* sometimes showed a weaker response (e.g. *DREB1C*) or a stronger response (e.g. *RD29A*). Curiously, the most striking observation was the correlation between increased m^{6}A in *mta*, compared to WT, with increased turnover and translation for a range of transcripts including *COR47*, *KIN1*, *COR413*, *COR15A*, *DREB1A*, and *DREB1B*. In the case of these transcripts, which were hypomethylated during DT in both genotypes, there was a more pronounced reduction in RNA turnover and translation under DT. This suggests that m^{6}A may have the most pronounced effect on the regulation of these transcripts, while also highlighting the complexity of disentangling m^{6}A-mediated regulation from that of stress-signaling pathways.

Discussion

Covalent RNA modifications such as m^{6}A have been linked to multiple aspects of RNA regulation including processing, stability, and translation. In plants, stress-induced changes in m^{6}A have been associated with proper stress response (Hu *et al.*, 2021; Martínez-Pérez *et al.*, 2021; Govindan *et al.*, 2022; Zhang *et al.*, 2022; Prall *et al.*, 2023b). An analysis of the role of MTA-dependent m^{6}A regulation during drought, a significant stressor that affects grain and fodder production, has yet to be investigated. Here, we demonstrate that MTA, the catalytic subunit of the major m^{6}A methyltransferase, is important for drought tolerance in Arabidopsis. We find that drought repatterns m^{6}A across thousands of transcripts in a largely MTA-dependent manner, alongside evidence of possible compensatory m^{6}A regulation when MTA is disrupted. Critically, changes at MTA-affected sites were tied to drought-responsive mRNA regulation. Our analysis also suggests that MTA has m^{6}A-independent impacts on mRNA regulation, warranting caution of the extent to which we assign regulatory potential to m^{6}A.

We demonstrate that plants lacking MTA are drought-sensitive (Fig. 1). This aligns with work showing *mta* to be susceptible to variable abiotic factors, including cold, salt, copper-induced oxidative stress, and high light (Hu *et al.*, 2021; Govindan *et al.*, 2022; Zhang *et al.*, 2022; Sharma *et al.*, 2024). Contrastingly, *mta* has improved pathogen resistance (Martínez-Pérez *et al.*, 2021; Prall *et al.*, 2023b). This dichotomy suggests that MTA, or m^{6}A reader proteins, may have condition-specific effects and/or regulation. For example, ECT2/3/4 stabilizes m^{6}A-modified mRNAs encoding ABA signaling proteins (Song *et al.*, 2023). Contrarily, ECT8 inhibits translation of m^{6}A-modified ABA-related transcripts during drought (Wu *et al.*, 2024). Despite such complexities, these observations reinforce m^{6}A as an important component of gene regulation during stress.

We observe a predominantly MTA-dependent global increase in m^{6}A during drought in the 3′ UTR of transcripts related to metabolism, gene regulation, and stress response (Fig. 2a,d,e). However, an MTA-independent increase occurred in the 5′ UTR, albeit representing a small number of sites. This aligns with a global increase in m^{6}A that was observed in Arabidopsis under high light at the 3′ end of transcripts related to photosynthesis and RNA regulation (Zhang *et al.*, 2022). This process was perturbed in *vir-1* mutants, again implicating the major m^{6}A methyltransferase complex (Zhang *et al.*, 2022). Similarly, FIO1 was found to methylate *c.* 1000 salt-inducible transcripts to facilitate salt tolerance (Cai *et al.*, 2024). Contrastingly, cold and pathogen stress lead to reduced m^{6}A in the 3′ UTR (Govindan *et al.*, 2022; Prall *et al.*, 2023b). Interestingly, reduction of m^{6}A during infection may involve the m^{6}A eraser, ALKBH10B, at defense-related transcripts (Prall *et al.*, 2023b). These findings highlight the condition- and transcript-specific nature of m^{6}A dynamics, possibly underpinned by differential regulation of the m^{6}A writing and erasing machinery.

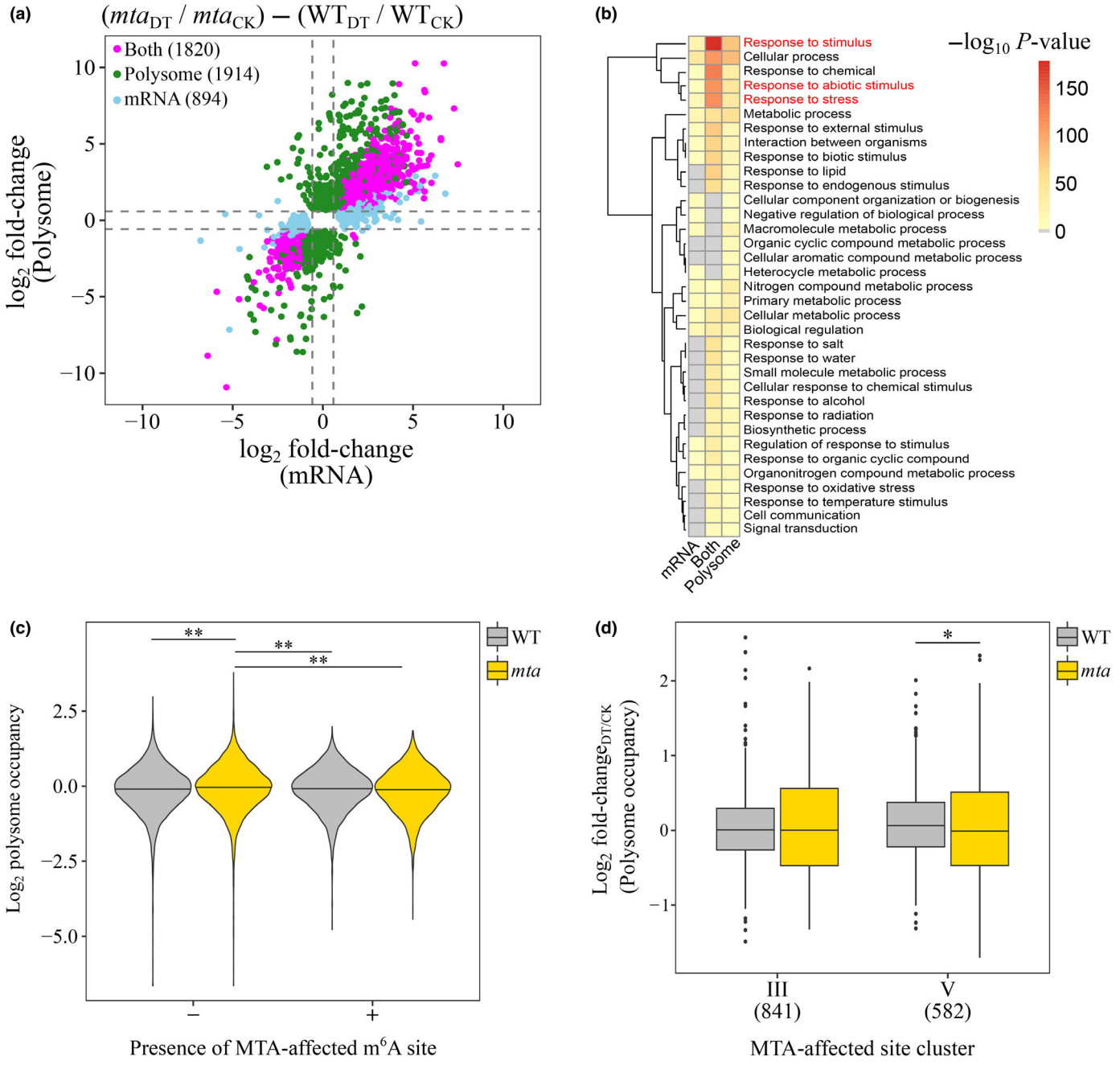

Fig. 5 mRNA ADENOSINE METHYLASE (MTA) and m^{6}A impact DT-responsive regulation of polysome occupancy in Arabidopsis. (a, b) Scatter plot of changes in polysomal and input mRNA (a), and over-represented GO terms (b), for genes with differential DT response in *mta*. Colours denote statistically significant changes in input mRNA (blue), polysomal mRNA (green), or both (magenta). (c) Violin plot of $\log_2$ proportion uncapped in wild-type (WT) and *mta* (CK only) for transcripts with (+) or without (–) a MTA-affected m^{6}A site. Horizontal line denotes median. (d) Standard boxplots of $\log_2$ fold-changes in polysome occupancy during DT, in WT and *mta*, for transcripts contain a MTA-affected m^{6}A site from Cluster III or V. Numbers denote the number of genes detected for each category. Statistical significance was determined using Dunn's test of multiple comparisons with *P*-values adjusted using the Bonferroni method: **, $P < 0.01$; *, $P < 0.05$.

m^{6}A can directly inhibit endonucleolytic mRNA cleavage (Anderson *et al.*, 2018) and influence RNA-protein binding (Wang *et al.*, 2014; Zhu *et al.*, 2014). It is, therefore, unsurprising that m^{6}A can have contrasting effects on mRNA regulation. Under steady state, m^{6}A had the most notable impact on mRNA abundance and stability (Figs 3c, 4c). Although it is unclear what is cause and effect, since there were negligible differences between WT and *mta* for transcripts harboring MTA-dependent m^{6}A sites. Furthermore, amongst transcripts with MTA-affected m^{6}A sites, the only relationship observed was a modest negative correlation with mRNA abundance (Pearson's $r = -0.49$) (Fig. S3). Interestingly, this relationship between m^{6}A and

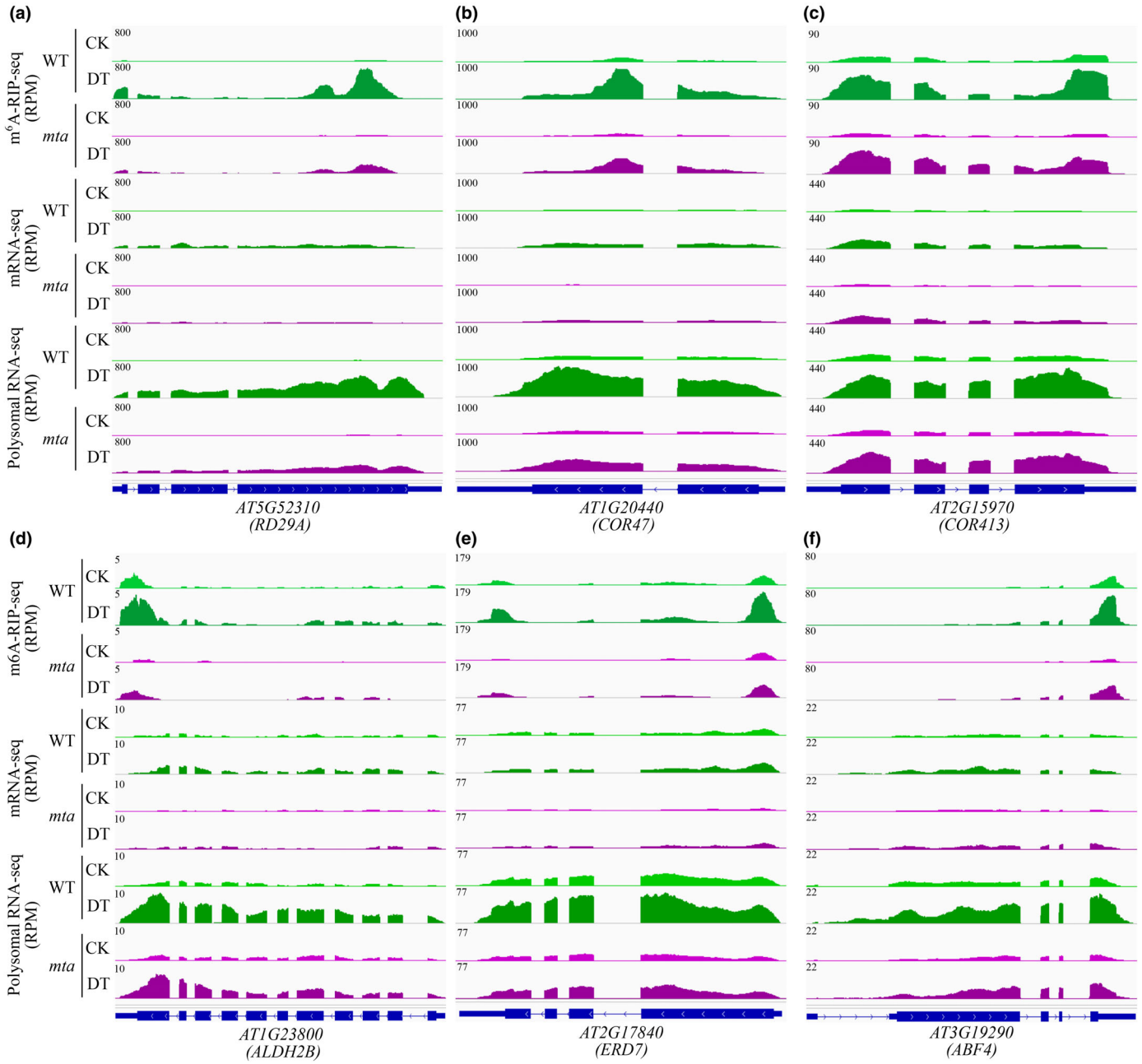

Fig. 6 Genome browser examples of drought-related transcripts. Genome browser shots of m^{6}A-IP-seq, mRNA-seq, and polysomal RNA-seq for exemplar drought-related genes that show regulation by m6A: (a) *RD29A*, (b) *COR47*, (c) *COR413*, (d) *ALDH2B*, (e) *ERD7*, and (f) *ABF4*.

mRNA abundance was also observed in maize lines B73 (Pearson's $r = -0.66$) and Mo17 (Pearson's $r = -0.65$) (Luo *et al.*, 2020). The limited relationships observed may reflect compensatory regulation in *mta* that counteracts m^{6}A-dependent effects when unperturbed.

Contrarily, the impacts of m^{6}A on mRNA regulation appear to be more pronounced during stress (Anderson *et al.*, 2018; Hu *et al.*, 2021; Govindan *et al.*, 2022; Zhang *et al.*, 2022; Prall *et al.*, 2023b; Sharma *et al.*, 2024). Despite an overall reduction in m^{6}A, stress-induced increases in m^{6}A in *mta* were still prevalent (Fig. 2c), which we hypothesize reflects compensatory activity by other m^{6}A regulators. However, such a phenomenon has yet to be described and requires measuring m^{6}A levels in higher order mutants of the relevant methyltransferases and/or demethylases. Nonetheless, this complexity allowed us to contrast sites with (Cluster V) and without (Cluster III) MTA-dependent changes. Using this method, we associated MTA-dependent increases in m^{6}A with decreased abundance (Fig. 3d), decreased stability (Fig. 4f) and increased translation (Fig. 5d) for *c.* 586 transcripts, related to metabolism and gene regulation, during drought. Comparisons to other studies highlight the context-dependent impacts of m^{6}A. For example, flagellin 22 (a fragment

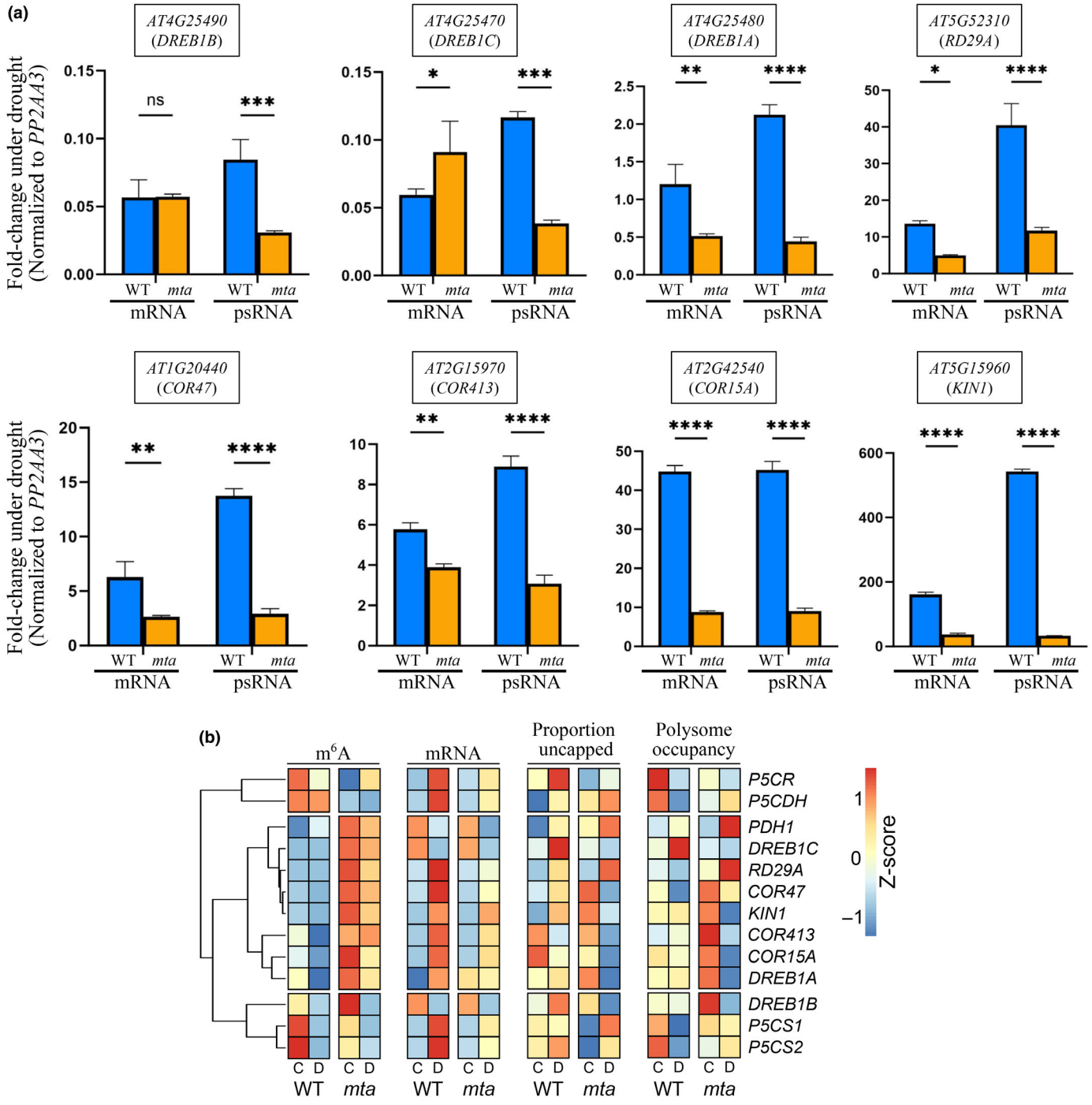

Fig. 7 Translational regulation of drought-related transcripts is impaired in *mta* and correlates with reduced m^{6}A in Arabidopsis. (a) Fold-change in abundance of select drought-related genes under DT in total mRNA (mRNA) and polysomal RNA (psRNA) fractions as determined by reverse transcription quantitative polymerase chain reaction. Expression changes were normalized against PP2AA3 (AT1G13320). Data are shown as mean and SD. Statistical significance denoted by: *, $P < 0.05$; **, $P < 0.01$; ***, $P < 0.001$; ****, $P < 0.0001$. (b) Heatmaps with one-dimensional hierarchical clustering of rows representing m^{6}A enrichment, mRNA abundance, proportion of uncapped transcripts, and polysome occupancy for select drought-related genes. Values represent row-wise Z-scores for each metric.

of bacterial flagellin) treatment led to reduced m^{6}A in the 3′ UTR, which was associated with increased stability and abundance of 144 defense-related transcripts (Prall *et al.*, 2023b). On the other hand, m^{6}A was positively correlated with transcript stability during salt stress (Cai *et al.*, 2024). During strawberry fruit ripening, m^{6}A was positively correlated with increased stability for two ABA-related transcripts and five transcripts encoding translation factors (Zhou *et al.*, 2021). In maize, increased m^{6}A at the start codon was linked with higher translation; however, heavy m^{6}A in the 3′ UTR was associated with reduced

translation (Luo *et al.*, 2020). These contrasting observations reinforce the need for a context-dependent understanding of m^{6}A-dependent mRNA regulation, including the regulation and activities of m^{6}A reader proteins such as the ECTs.

Drought susceptibility of *mta* is likely a consequence of improper regulation of key drought responders such as *DREB1A/B/C*, *COR47/413*, and *RD29A* (Figs 6, 7). Our targeted analysis showed a positive correlation between m^{6}A and translation for *COR413*, *COR47*, *RD29A*, *ERD7*, *ALDH2B*, and *ABF4* (Fig. 6). Similar observations were made during cold stress, where m^{6}A promoted the translation of *COR47* and *COR413* (Govindan *et al.*, 2022). Impaired translation of *DREB1A/B/C* could impact the transcription of *c.* 6000 target genes (Song *et al.*, 2021). Consistent with this, multiple DREB targets (*RD29A*, *COR47*, *COR413*, *COR15A*, and *KIN1*) were significantly lower in *mta*, compared with WT, under drought (Figs 6, 7). This aligns with the observation of substantial changes in drought-responsive mRNA regulation in *mta*, especially for stress-responsive transcripts (Figs 3a,b, 4c,d, 5a,b). The breadth of impacts observed in *mta* raises the possibility of m^{6}A-independent effects. Indeed, crosstalk between MTA and RNA Polymerase II (RNAPII) could affect the pool of transcripts available for methylation. In human cells, attenuated RNAPII transcription was linked to higher m^{6}A and reduced translation (Slobodin *et al.*, 2017). In plants, interaction between MTA and RNAPII was demonstrated in the context of miRNA biogenesis (Bhat *et al.*, 2020). In addition, Bhat *et al.* (2023) show that m^{6}A-modified transcripts during cold stress had higher RNAPII occupancy. Lack of MTA disrupted RNAPII elongation, which impaired cold-responsive gene regulation (Bhat *et al.*, 2023). Transcription and mRNA decay are coupled processes, whereby decay factors can shuttle between the nucleus and cytoplasm to synchronize decay rates with the transcription of a given mRNA (Chattopadhyay *et al.*, 2022). Newly synthesized mRNAs can also be cotranscriptionally 'imprinted' in the nucleus, which can influence its export, decay, and translation (Dahan & Choder, 2013). Additionally, disruption of RNAPII termination has also been associated with a global increase in uncapped RNAs (Crisp *et al.*, 2018). It is possible RNAPII dynamics are impaired in the absence of MTA, which may influence mRNA stability through a similar process, as described above, providing a potential mechanism of m^{6}A-independent impacts of MTA on mRNA regulation. However, such findings should not negate the importance of m^{6}A. For example, an Arabidopsis line expressing catalytically inactive FIO1 had reduced salt tolerance (Cai *et al.*, 2024). Similarly, expression of catalytically inactive MTA resulted in impaired *MIR393b* biogenesis (Bhat *et al.*, 2020). Therefore, drought-specific changes in m^{6}A at a subset of transcripts could profoundly impact drought tolerance. Taken together, we conclude that MTA is important for drought tolerance in Arabidopsis through both m^{6}A-dependent and -independent effects on mRNA regulation.

Acknowledgements

We thank members of the BDG and RS labs, both past and present, for helpful discussions. We thank Wil Prall for critical feedback and suggestions. This work was funded by NSF grant IOS-2023310 to BDG, IOS-1849708 to BDG and RS, and NSF-EPSCoR RII Track-2 FEC-1826836 as well as Stevens Endowed Chair to RS.

Competing interests

None declared.

Author contributions

RS and BDG conceived and designed the study. YL performed drought assay and polysomal RNA-sequencing. ST and PJN conducted phenotypic and physiological analysis. SSB performed m^{6}A-RIP-sequencing. DRG performed GMUCT. DRG and BDG analyzed the datasets. DRG, SSB, BDG and RS interpreted the data. DRG and SSB wrote the manuscript. RS and BDG reviewed and edited the manuscript. DRG and YL contributed equally to this work.

ORCID

Susheel Sagar Bhat https://orcid.org/0000-0001-9227-6466
Diep R. Ganguly https://orcid.org/0000-0001-6746-0181
Brian D. Gregory https://orcid.org/0000-0001-7532-0138
Ramanjulu Sunkar https://orcid.org/0000-0002-2012-1526

Data availability

All sequencing data are accessible under NCBI accession no. GSE243365.

References

Anderson SJ, Kramer MC, Gosai SJ, Yu X, Vandivier LE, Nelson ADL, Anderson ZD, Beilstein MA, Fray RG, Lyons E *et al.* 2018. N-methyladenosine inhibits local ribonucleolytic cleavage to stabilize mRNAs in Arabidopsis. *Cell Reports* **25**: 1146–1157.

Arribas-Hernández L, Bressendorff S, Hansen MH, Poulsen C, Erdmann S, Brodersen P. 2018. An mA-YTH module controls developmental timing and morphogenesis in Arabidopsis. *Plant Cell* **30**: 952–967.

Arribas-Hernández L, Brodersen P. 2020. Occurrence and functions of mA and other covalent modifications in plant mRNA. *Plant Physiology* **182**: 79–96.

Bartels D, Sunkar R. 2005. Drought and salt tolerance in plants. *Critical Reviews in Plant Sciences* **24**: 23–58.

Bechtold U, Field B. 2018. Molecular mechanisms controlling plant growth during abiotic stress. *Journal of Experimental Botany* **69**: 2753–2758.

Bhat SS, Bielewicz D, Gulanicz T, Bodi Z, Yu X, Anderson SJ, Szewc L, Bajczyk M, Dolata J, Grzelak N *et al.* 2020. mRNA adenosine methylase (MTA) deposits mA on pri-miRNAs to modulate miRNA biogenesis in. *Proceedings of the National Academy of Sciences, USA* **117**: 21785–21795.

Bhat SS, Bielewicz D, Kindgren P. 2023. MTA influences RNA polymerase II transcription dynamics and regulates the cold response in Arabidopsis. *bioRxiv*. doi: 10.1101/2023.05.10.540235.

Bodi Z, Zhong S, Mehra S, Song J, Graham N, Li H, May S, Fray RG. 2012. Adenosine methylation in Arabidopsis mRNA is associated with the 3′ end and reduced levels cause developmental defects. *Frontiers in Plant Science* **3**: 48.

Cai J, Hu J, Xu T, Kang H. 2024. FIONA1-mediated mRNA mA methylation regulates the response of Arabidopsis to salt stress. *Plant, Cell & Environment* **47**: 900–912.

Carillo P, Yves G. 2011. *Extraction and determination of proline.* PrometheusWiki. [WWW document] URL https://prometheusprotocols.net/ [accessed 28 August 2023].

Chan KX, Phua SY, Crisp P, McQuinn R, Pogson BJ. 2016. Learning the languages of the chloroplast: retrograde signaling and beyond. *Annual Review of Plant Biology* **67**: 25–53.

Chattopadhyay S, Garcia-Martinez J, Haimovich G, Fischer J, Khwaja A, Barkai O, Chuartzman SG, Schuldiner M, Elran R, Rosenberg MI *et al.* 2022. RNA-controlled nucleocytoplasmic shuttling of mRNA decay factors regulates mRNA synthesis and a novel mRNA decay pathway. *Nature Communications* **13**: 7184.

Chen X, Ding Y, Yang Y, Song C, Wang B, Yang S, Guo Y, Gong Z. 2021. Protein kinases in plant responses to drought, salt, and cold stress. *Journal of Integrative Plant Biology* **63**: 53–78.

Crisp PA, Smith AB, Ganguly DR, Murray KD, Eichten SR, Millar AA, Pogson BJ. 2018. RNA polymerase II read-through promotes expression of neighboring genes in SAL1-PAP-XRN retrograde signaling. *Plant Physiology* **178**: 1614–1630.

Dahan N, Choder M. 2013. The eukaryotic transcriptional machinery regulates mRNA translation and decay in the cytoplasm. *Biochimica et Biophysica Acta* **1829**: 169–173.

Duan H-C, Wei L-H, Zhang C, Wang Y, Chen L, Lu Z, Chen PR, He C, Jia G. 2017. ALKBH10B is an RNA-methyladenosine demethylase affecting Arabidopsis floral transition. *Plant Cell* **29**: 2995–3011.

Ganguly DR, Hickey LT, Crisp PA. 2022. Harnessing genetic variation at regulatory regions to fine-tune traits for climate-resilient crops. *Molecular Plant* **15**: 222–224.

Govindan G, Sharma B, Li Y-F, Armstrong CD, Merum P, Rohila JS, Gregory BD, Sunkar R. 2022. mRNA N-methyladenosine is critical for cold tolerance in Arabidopsis. *The Plant Journal* **111**: 1052–1068.

Hou C-Y, Lee W-C, Chou H-C, Chen A-P, Chou S-J, Chen H-M. 2016. Global analysis of truncated RNA ends reveals new insights into ribosome stalling in plants. *Plant Cell* **28**: 2398–2416.

Hu J, Cai J, Park SJ, Lee K, Li Y, Chen Y, Yun J-Y, Xu T, Kang H. 2021. N-methyladenosine mRNA methylation is important for salt stress tolerance in Arabidopsis. *The Plant Journal* **106**: 1759–1775.

Kierzek E, Kierzek R. 2003. The thermodynamic stability of RNA duplexes and hairpins containing N6-alkyladenosines and 2-methylthio-N6-alkyladenosines. *Nucleic Acids Research* **31**: 4472–4480.

Kramer MC, Janssen KA, Palos K, Nelson ADL, Vandivier LE, Garcia BA, Lyons E, Beilstein MA, Gregory BD. 2020. N-methyladenosine and RNA secondary structure affect transcript stability and protein abundance during systemic salt stress in Arabidopsis. *Plant Direct* **4**: e00239.

Lee W-C, Hou B-H, Hou C-Y, Tsao S-M, Kao P, Chen H-M. 2020. Widespread exon junction complex footprints in the RNA degradome mark mRNA degradation before steady state translation. *Plant Cell* **32**: 904–922.

Li Y-F, Mahalingam R, Sunkar R. 2017. Isolation of polysomal RNA for analyzing stress-responsive genes regulated at the translational level in plants. *Methods in Molecular Biology* **1631**: 151–161.

Liu N, Dai Q, Zheng G, He C, Parisien M, Pan T. 2015. N(6)-methyladenosine-dependent RNA structural switches regulate RNA-protein interactions. *Nature* **518**: 560–564.

Liu N, Zhou KI, Parisien M, Dai Q, Diatchenko L, Pan T. 2017. N6-methyladenosine alters RNA structure to regulate binding of a low-complexity protein. *Nucleic Acids Research* **45**: 6051–6063.

Livak KJ, Schmittgen TD. 2001. Analysis of relative gene expression data using real-time quantitative PCR and the 2(-Delta Delta C(T)) method. *Methods* **25**: 402–408.

Luo G-Z, MacQueen A, Zheng G, Duan H, Dore LC, Lu Z, Liu J, Chen K, Jia G, Bergelson J *et al.* 2014. Unique features of the m6A methylome in *Arabidopsis thaliana*. *Nature Communications* **5**: 5630.

Luo J-H, Wang Y, Wang M, Zhang L-Y, Peng H-R, Zhou Y-Y, Jia G-F, He Y. 2020. Natural variation in RNA mA methylation and its relationship with translational status. *Plant Physiology* **182**: 332–344.

Martínez-Pérez M, Gómez-Mena C, Alvarado-Marchena L, Nadi R, Micol JL, Pallas V, Aparicio F. 2021. The mA RNA demethylase ALKBH9B plays a critical role for vascular movement of alfalfa mosaic virus in Arabidopsis. *Frontiers in Microbiology* **12**: 745576.

Mi H, Muruganujan A, Huang X, Ebert D, Mills C, Guo X, Thomas PD. 2019. Protocol update for large-scale genome and gene function analysis with the PANTHER classification system (v.14.0). *Nature Protocols* **14**: 703–721.

Mickelbart MV, Hasegawa PM, Bailey-Serres J. 2015. Genetic mechanisms of abiotic stress tolerance that translate to crop yield stability. *Nature Reviews. Genetics* **16**: 237–251.

Mielecki D, Zugaj DŁ, Muszewska A, Piwowarski J, Chojnacka A, Mielecki M, Nieminuszczy J, Grynberg M, Grzesiuk E. 2012. Novel AlkB dioxygenases—alternative models for in silico and *in vivo* studies. *PLoS ONE* 7: e30588.

Prall W, Ganguly DR, Gregory BD. 2023a. The covalent nucleotide modifications within plant mRNAs: what we know, how we find them, and what should be done in the future. *Plant Cell* **35**: 1801–1816.

Prall W, Sheikh AH, Bazin J, Bigeard J, Almeida-Trapp M, Crespi M, Hirt H, Gregory BD. 2023b. Pathogen-induced m6A dynamics affect plant immunity. *Plant Cell* **35**: 4155–4172.

Ramanjulu S, Bartels D. 2002. Drought- and desiccation-induced modulation of gene expression in plants. *Plant, Cell & Environment* **25**: 141–151.

Ramanjulu S, Sudhakar C. 2000. Proline metabolism during dehydration in two mulberry genotypes with contrasting drought tolerance. *Journal of Plant Physiology* **157**: 81–85.

Razzaq A, Wani SH, Saleem F, Yu M, Zhou M, Shabala S. 2021. Rewilding crops for climate resilience: economic analysis and *de novo* domestication strategies. *Journal of Experimental Botany* **72**: 6123–6139.

Reichel M, Köster T, Staiger D. 2019. Marking RNA: m6A writers, readers, and functions in Arabidopsis. *Journal of Molecular Cell Biology* **11**: 899–910.

Růžička K, Zhang M, Campilho A, Bodi Z, Kashif M, Saleh M, Eeckhout D, El-Showk S, Li H, Zhong S *et al.* 2017. Identification of factors required for m A mRNA methylation in Arabidopsis reveals a role for the conserved E3 ubiquitin ligase HAKAI. *New Phytologist* **215**: 157–172.

Scutenaire J, Deragon J-M, Jean V, Benhamed M, Raynaud C, Favory J-J, Merret R, Bousquet-Antonelli C. 2018. The YTH domain protein ECT2 is an mA reader required for normal trichome branching in Arabidopsis. *Plant Cell* **30**: 986–1005.

Sharma B, Govindan G, Li Y, Sunkar R, Gregory BD. 2024. RNA N6-methyladenosine affects copper-induced oxidative stress response in *Arabidopsis thaliana*. *Non-Coding RNA* **10**: 8.

Shen L, Liang Z, Gu X, Chen Y, Teo ZWN, Hou X, Cai WM, Dedon PC, Liu L, Yu H. 2016. N(6)-methyladenosine RNA modification regulates shoot stem cell fate in Arabidopsis. *Developmental Cell* **38**: 186–200.

Slobodin B, Han R, Calderone V, Vrielink JAFO, Loayza-Puch F, Elkon R, Agami R. 2017. Transcription impacts the efficiency of mRNA translation via co-transcriptional N6-adenosine methylation. *Cell* **169**: 326–337.

Song P, Wei L, Chen Z, Cai Z, Lu Q, Wang C, Tian E, Jia G. 2023. mA readers ECT2/ECT3/ECT4 enhance mRNA stability through direct recruitment of the poly(A) binding proteins in Arabidopsis. *Genome Biology* **24**: 103.

Song Y, Zhang X, Li M, Yang H, Fu D, Lv J, Ding Y, Gong Z, Shi Y, Yang S. 2021. The direct targets of CBFs: in cold stress response and beyond. *Journal of Integrative Plant Biology* **63**: 1874–1887.

Sun B, Bhati KK, Song P, Edwards A, Petri L, Kruusvee V, Blaakmeer A, Dolde U, Rodrigues V, Straub D *et al.* 2022. FIONA1-mediated methylation of the 3′UTR of FLC affects FLC transcript levels and flowering in Arabidopsis. *PLoS Genetics* **18**: e1010386.

Sunkar R, Li Y-F, Jagadeeswaran G. 2012. Functions of microRNAs in plant stress responses. *Trends in Plant Science* **17**: 196–203.

Vandivier LE, Campos R, Kuksa PP, Silverman IM, Wang L-S, Gregory BD. 2015. Chemical modifications mark alternatively spliced and uncapped messenger RNAs in Arabidopsis. *Plant Cell* **27**: 3024–3037.

Vandivier LE, Gregory BD. 2018. New insights into the plant epitranscriptome. *Journal of Experimental Botany* **69**: 4659–4665.

Wang C, Yang J, Song P, Zhang W, Lu Q, Yu Q, Jia G. 2022. FIONA1 is an RNA N-methyladenosine methyltransferase affecting Arabidopsis photomorphogenesis and flowering. *Genome Biology* **23**: 40.

Wang X, Lu Z, Gomez A, Hon GC, Yue Y, Han D, Fu Y, Parisien M, Dai Q, Jia G *et al.* 2014. N6-methyladenosine-dependent regulation of messenger RNA stability. *Nature* **505**: 117–120.

Wei L-H, Song P, Wang Y, Lu Z, Tang Q, Yu Q, Xiao Y, Zhang X, Duan H-C, Jia G. 2018. The mA reader ECT2 controls trichome morphology by affecting mRNA stability in Arabidopsis. *Plant Cell* **30**: 968–985.

Willmann MR, Berkowitz ND, Gregory BD. 2014. Improved genome-wide mapping of uncapped and cleaved transcripts in eukaryotes – GMUCT 2.0. *Methods* **67**: 64–73.

Wu X, Su T, Zhang S, Zhang Y, Wong CE, Ma J, Shao Y, Hua C, Shen L, Yu H. 2024. N-methyladenosine-mediated feedback regulation of abscisic acid perception via phase-separated ECT8 condensates in Arabidopsis. *Nature Plants* **10**: 469–482.

Xu T, Wu X, Wong CE, Fan S, Zhang Y, Zhang S, Liang Z, Yu H, Shen L. 2022. FIONA1-mediated mA modification regulates the floral transition in Arabidopsis. *Advancement of Science* **9**: e2103628.

Yamaguchi-Shinozaki K, Shinozaki K. 2006. Transcriptional regulatory networks in cellular responses and tolerance to dehydration and cold stresses. *Annual Review of Plant Biology* **57**: 781–803.

Yu X, Willmann MR, Anderson SJ, Gregory BD. 2016. Genome-wide mapping of uncapped and cleaved transcripts reveals a role for the nuclear mRNA cap-binding complex in cotranslational RNA decay in Arabidopsis. *Plant Cell* **28**: 2385–2397.

Zhang M, Zeng Y, Peng R, Dong J, Lan Y, Duan S, Chang Z, Ren J, Luo G, Liu B *et al.* 2022. N-methyladenosine RNA modification regulates photosynthesis during photodamage in plants. *Nature Communications* **13**: 7441.

Zhou L, Tang R, Li X, Tian S, Li B, Qin G. 2021. N-methyladenosine RNA modification regulates strawberry fruit ripening in an ABA-dependent manner. *Genome Biology* **22**: 168.

Zhu J-K. 2016. Abiotic stress signaling and responses in plants. *Cell* **167**: 313–324.

Zhu T, Roundtree IA, Wang P, Wang X, Wang L, Sun C, Tian Y, Li J, He C, Xu Y. 2014. Crystal structure of the YTH domain of YTHDF2 reveals mechanism for recognition of N6-methyladenosine. *Cell Research* **24**: 1493–1496.

Supporting Information

Additional Supporting Information may be found online in the Supporting Information section at the end of the article.

Fig. S1 m^6A-RIP-sequencing quality control.

Fig. S2 Profiling drought-responsive changes in mRNA abundance in *mta*.

Fig. S3 Correlation of m^6A with mRNA abundance, proportion of uncapped RNAs, and polysome occupancy.

Fig. S4 Global increase in uncapped RNA under drought and in *mta*.

Fig. S5 Profiling changes in polysome-associated RNA in *mta*.

Methods S1 Sequencing analyses.

Table S1 Primers used for reverse transcription quantitative polymerase chain reaction.

Table S2 Sequencing dataset summary.

Table S3 High-confidence m6A peaks identified in each sample group.

Table S4 mRNA ADENOSINE METHYLASE-affected m6A sites and overlapping transcripts.

Table S5 Differential expression analysis using input mRNA samples.

Table S6 Differential expression analysis using global mapping of uncapped and cleaved transcripts samples.

Table S7 Log_2 fold-changes in proportion uncapped RNA for transcripts harboring mRNA ADENOSINE METHYLASE-affected m6A sites.

Table S8 Differential expression analysis using polysomal RNA samples.

Table S9 Log_2 fold-changes in polysome occupancy for transcripts harboring mRNA ADENOSINE METHYLASE-affected m^6A sites.

Please note: Wiley is not responsible for the content or functionality of any Supporting Information supplied by the authors. Any queries (other than missing material) should be directed to the *New Phytologist* Central Office.